Effects of Shear Flow on the Stability of Tokamak Plasmas
Extended abstract

Author: Josué Lopes
Under the supervision of Dr. R. Coelho and Dr. E. Westerhof
(Dated: May 2018)

Tearing modes may be a major performance limiting player in *tokamak* magnetic confinement. The linear evolution of the classical tearing mode is investigated here with a numerical modelling single helicity reduced MHD code. Results are compared to the theoretical predictions for dispersion relations, the stabilizing effect of perfectly conducting walls at the boundaries, as well as the stabilizing effect of finite viscosity. Shear flow is found to have either stabilizing or destabilizing effect, depending on the ratio of rotation shear layer width to the current density layer width. Below a certain threshold ratio, which depends on the Prandtl number, shear flow is stabilizing and above that threshold, the opposite is observed. Furthermore, the stabilizing/destabilizing effect is much more notorious in the two limiting cases: inviscid and strongly viscous regimes. The results suggest that shear flow has a destabilizing effect in the outer layer and a stabilizing effect on the inner layer. Marginally stable modes fail to be destabilized in the presence of shear flow when shear is supposedly a destabilizing effect.

I. INTRODUCTION

There is an urgent need of finding new ways to produce clean and cheap energy [1]. In the 1950's, soviet scientists designed a device called *tokamak* which could provide the solution to this problem. By fusing one gram of Deuterium and Tritium, (hydrogen isotopes used as fuels) 9×10^{13} Joules are released [2]. Inside a *tokamak*, the fusion fuel, in the state called plasma is confined by using the plasma's magnetic proprieties and is characterized by a set of toroidal and poloidal coils that generates closed helical field lines around the torus. This topology confines the particles and is widely considered the most promising concept towards a fusion power plant.

In a plasma with toroidal axisymmetry, the total magnetic field is distributed and aligned inside the torus in such a way that they are tangent to nested toroidal surfaces, designated by magnetic surfaces. These surfaces shape and position characterize how the magnetic equilibrium is established. The two major obstacles to higher confinement are turbulent transport and plasma instabilities.

Plasma instabilities may be divided into two general categories: magnetohydrodynamic (MHD) and kinetic instabilities. The former may pose the most stringent limitations to plasma performance and detrimental effects on plasma confinement, and are described by a MHD model of the plasma. The tearing mode is a resistive mode characterized by topological change ("*the tear*") of the flux surfaces and formation of magnetic islands as observed in Figure 1. It is considered responsible for major plasma disruptions (a sudden termination of the plasma) [3].

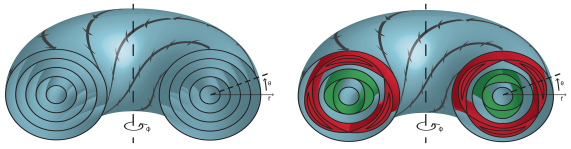

Figure 1: On the left, the set of nested flux surfaces compose the ideal magnetic topology. On the right, the q=m/n=2 and q=m/n=3 surfaces are broken up and reconnected, resulting in q=2/1 (green) and q=3/1 (red) islands. A circular cross-section approximation was considered and the thick black arrows on the most outer surface represent the closed helical magnetic field lines.

Turbulent transport can be seen as turbulent cells in the plasma where the transport is greatly enhanced. Sheared flow (i.e. different velocity at each radial point) shreds these turbulent cells reducing their size and consequently the transport is reduced [4]. Shear flow is now a widely accepted suppression mechanism of turbulent transport.

This document aims to understand whether the effect of shear flow can also stabilize tearing modes. For this investigation, a revision of the most relevant literature is presented in section II, followed by the MHD model that characterizes the evolution of the tearing mode in section III. The developments to the numerical code are very briefly explained in section IV and the benchmark of the numerical results

with the theoretical predictions are conferred in section V. Finally the effects of shear flow are discussed in section VI, followed by the main conclusion of this work.

II. BACKGROUND

The physical picture of a tearing mode can be understood by considering a sheet pinch configuration. A sheared equilibrium magnetic field will change sign in the helical direction which is perpendicular to the equilibrium field lines at the resonant surface (r_s) q=m/n (here the field lines close onto themselves after m poloidal and n toroidal turns). In a perfectly conducting plasma, the magnetic field lines are not allowed to stream past fluid element. With the addition of a perturbation perpendicular to the equilibrium magnetic field, the flux outside a constant flux surface of fixed area changes. This flux change, characterized by the slipping of the field line with respect to the fluid element, is forbidden and must be corrected by the appearance of eddy currents δj_z, which will be sharply peaked for small x=r-r_s. However, with a finite resistivity, this restoring force, is no longer infinite [5]. Thus the superposition of the perturbed magnetic field with the equilibrium magnetic field outlines the tearing and reconnection of the magnetic field lines in a configuration of magnetic islands, shown in Figure 2.

The radial magnetic field perturbation growing with growth rate γ induces a current j_{z1} in the toroidal direction which provides the x-direction linear forces $-j_z B_y$ indicated in Figure 2. These drive the flow pattern of narrow vortices which are also shown. Moving away from the resistive singular layer, the induced electric field produces a flow v_x = -E_z/B_y and for an incompressible flow (due to a strong equilibrium field in the toroidal direction), this requires a strongly sheared flow in the y-direction over the layer (the vortex pattern shown).

Magnetic reconnection occurs when the plasma is forced towards a resistive layer, where resistive diffusion becomes non-negligible and the magnetic field changes sign [6]. As a result, an x-point appears inside the resistive layer and the field lines are reconnected, following the plasma flow in along the sides and out along the upper and lower sides with respect to the x-point (see single arrows near the vortices in Figure 2). With the magnetic field oriented in the four regions delimited by the x-point and the separatrix, a thin boundary layer will form

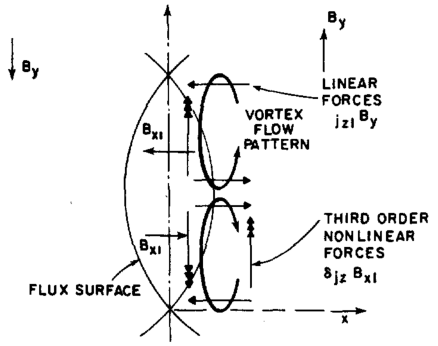

Figure 2: Tearing mode structure inside the singular layer. The magnetic field perturbation in the radial direction superimposed to the equilibrium field produces flux surfaces, forming the structure shown, and are entitled by magnetic islands. The separatrix is surface of constant flux, wich joins the island's x-points. The vortex flow carrying the plasma into the magnetic island is, in linear theory, driven against inertia by the linear forces $j_{z1}B_y$ indicated by single headed arrows. In the non-linear theory, second order y-independent eddy currents δj_z arise which produce third order forces $\delta j_z B_{x1}$, indicated by triple headed arrows, which oppose the vortex flow, and which replace the effect of the inertia as the mode grows [5].

between them, separating the plasmas and their respective magnetic fields. Due to the different orientations tangential to the boundary, the layer must also constitute a current sheet. Depending on the current direction, it will yield a positive or negative growth of the perturbation.

Furth, Killeen and Rosenbluth (1963) derived the tearing mode growth rate in slab geometry. They considered equations for the resistive current layer plane in the incompressible hydrodynamics approximation. The problem is divided in two regions: the resistive layer where finite conductivity allows relative fluid and field motion and the outer region where resistive diffusion is neglected. Thus the theory of tearing modes involves solving one set of equations in both regions and the complete eigenfunction requires a matching of the resulting solutions. The condition for matching determines the growth rate [7].

This condition is set by the stability parameter Δ' ("jump" in the logarithmic derivative of the perturbed magnetic flux across the inner layer) which translates to the available magnetic free energy in the plasma that is used to drive the island's growth. Consequently, one can tell that a negative stability parameter indicates that no instability will develop, unless additional effects drive the system.

When the island size becomes comparable to

the tearing layer width, non-linear effects start playing an important role. The y-independent eddy currents are reduced by the finite resistivity, however, the vortex flow will induce second order y-independent eddy currents δj_z. Then the y-direction third-order non-linear forces become non-negligible $\delta j_z B_x$ and provide a torque that opposes the vortex flow, as indicated in Figure 2. As the amplitude of these non-linear forces grow, they will replace the inertia as the dominant mechanism, opposing the growth of the mode. P. Rutherford [5] discovered that the island's growth is dramatically reduced; the exponential growth in time is replaced by algebraic growth on a much slower time scale. As the island width evolves in time, the non-linear modification of the equilibrium current density profile balances mode destabilization and a new magnetic equilibrium configuration with a saturated island is obtained [6].

Some important physical effects are responsible for altering the growth of the tearing mode. They are divided between effects that change the stability in the outer region (resistive wall interaction, mode coupling and externally imposed resonant magnetic fields) and inside the tearing layer (plasma pressure coupled with field line curvature and neo-classical bootstrap current):

Resistive wall interaction A magnetic island rotating with finite frequency induces an electric field in the conducting wall of the vessel, since the perturbed magnetic field of the island is time dependent. As a consequence, helical eddy currents induced in the wall give rise to a discontinuity in the derivative of the perturbed poloidal magnetic flux across the wall. The size of the discontinuity is proportional to the skin time of the wall and the frequency of the tearing mode, which imposes special boundary conditions on the perturbed magnetic flux and with it, the stability parameter of the mode changes. The existence of a resistive wall stabilizes the mode if the mode rotates ($w \neq 0$). Furthermore the resistive wall creates a drag torque which slows down the mode rotation. As the mode rotation decreases, the stabilizing effect and the electromagnetic torque that acts to slow down the island rotation are reduced [8]. When the mode's rotation reaches very low values, the mode is said to be locked to the wall and, in this case, the saturated width of the island is increased, and a disruption is likely to occur [9].

External Static Helical Magnetic Perturbation External fields which are resonant with the mode, have the same helicity - m,n. Considering that the external magnetic perturbation is produced by a thin helical winding located outside the plasma, the helical current flowing in the coil gives rise to a discontinuity in the derivative of the perturbed poloidal magnetic flux across the coil. This discontinuity is complex valued (depends on the phase difference between the mode and the external field) which is added to the non-interacting tearing mode stability parameter and is proportional to the strength of the interaction and the current flowing through the coil. A saturated mode that is free to lock to the external field is expected to be destabilizing (much like forced oscilator atractor), corresponding to a final larger saturated island width. On the other hand, a mode with slightly non-uniform rotation (not locked) gives rise to a net stabilizing effect on the mode [8].

Mode coupling When a plasma is confined in an arbitrary toroidal shape volume with a non-circular shape, the magnetic perturbations related to magnetic islands with different poloidal and toroidal mode numbers (m, n) haven't only a single (m,n) component, but also side band m$\pm$p harmonics (p$\in$ $\mathbb{N}$). In the non-linear growth of the mode, the perturbed flux and vorticity will couple different poloidal harmonics with the same toroidal mode number n. Therefore, the coupling between plasma perturbations with different wavenumber can occur when a magnetic perturbation with mode number (m,n) drives other perturbations with poloidal mode numbers m$\pm$p. As in the previously mentioned effect, the added term in the stability parameter is complex valued which depends on the phase difference between the mode and the other modes present in the plasma. Therefore, the complex contribution to the stability parameter from mode coupling, synchronizes the frequency of the coupled modes and favours their mutual destabilization [8, 10].

Plasma pressure associated with field line curvature In a toroidal geometry, plasma pressure and curvature (due to finite aspect ratio) effects give rise to a positive threshold for the stability parameter, below which the tearing mode is stable. In large devices, linear theory predicts that tearing modes are stable. Non-linearly, for some ranges of island width and plasma pressure radial derivative, the tearing modes become unstable. This means that a seed island that has a width surpassing a certain threshold will saturate at a width close to its saturation value in the absence of the stabilizing

curvature effects. For small island widths, the mode is stabilized. Furthermore, due to the 1/R dependency of the toroidal magnetic field, the curvature in the high-field side (at θ=π) is favourable since the magnetic field lines diverge from the plasma, in contrast to the low-field side where the opposite happens. Due to the poloidal dependency of the toroidal field, an overall positive curvature exists provided that the safety factor q>1. The curvature of the magnetic field and the pressure perturbation imply a perturbed parallel current density. This current density acts to reduce the stability parameter to an effective value which is the mentioned threshold from a stable to an unstable mode [11].

Neo-classical bootstrap current NTM is a high-β phenomenon, linearly stable ($\Delta' < 0$) and non-linearly unstable. The bootstrap current is a toroidal neoclassical effect that results from the radial pressure gradient, therefore proportional to β. An island of sufficient width can flatten locally the temperature, due to the rapid parallel transport along the field lines. As a result, the bootstrap current inside the island is removed while in the outer region the pressure gradient is maintained and so is the current. This local bootstrap current loss is equivalent to driving a helical current in the counter direction, easily shown to be destabilizing. Furthermore, R. Fitzpatrick [12] shows that only above a certain critical island width (W_d) does the mode experience the bootstarp effect since below W_d, the temperature is not fully flattened. The effects of bootstrap current alone are unlikely to destabilize a stable mode.

Local heating and current drive From the previous effect, if the local bootstrap current loss is replaced, the mode growth is reduced. Electron cyclotron radio-frequency heating (ECRH) and co-current drive through electron cyclotron current drive (ECCD) (in the direction of the equilibrium current) helps stabilizing a NTM. Heating inside the island separatrix (centred at the O-point) has an effect similar to driving a co-current since resistivity drops ($\eta \propto T^{-3/2}$) and the current is channelled in the direction of the equilibrium current. Provided that the current is driven in this direction, a more negative Δ' results [13].

III. MHD MODEL

A fluid model of the plasma may help to understand the phenomena related to instabilities, disruptions and magnetic reconnection. The magnetohydrodynamics model presented in this work includes Maxwell's equations for electric and magnetic fields and a plasma momentum balance equation. The equations were first derived in cylindrical geometry considering a large aspect ratio *tokamak* ($R_0/a \gg 1$ - major (R_0) and minor (a) radius) with circular cross section and a strongly magnetized plasma, narrowing down the MHD equations complexity into what is called the Reduced MHD. Thus, this work will focus on perturbations perpendicular to the equilibrium field lines, assuming that the helicity of this mode (m,n) matches the helicity of one flux surface in the chamber - the resonant surface.

The equations were then re-written in a slab geometry with a radial box size of length $L \ll a$. By unfolding the cylindrical layer around the magnetic island, the centre of the coordinate system will be placed at the rational surface where the magnetic island is excited. Here the slab's x-coordinate resembles the radial coordinate of a cylinder, defined as x=r-r_s and is bound to x $\in$ [-L,L] for $L \ll r_s$. The second coordinate z is parallel to the equilibrium magnetic field at the resonant surface (helical direction). The third coordinate y is perpendicular to the above coordinates follows the direction of the helical angle $\xi = \theta - n/(mR_0)z$ with a periodicity of 2π in respect to the azimuthal coordinate and a perimeter of $2\pi r_s$. Linearising this angle into a slab coordinate, leads to $dy = r_s d\xi$ and due to the periodicity of the angle $\xi \in [-\pi, \pi]$, the y coordinate will also have a periodicity of $2\pi r_s$ and $y \in [-r_s\pi,\ r_s\pi]$.

The perturbations take the form $f(x)\exp[i\,(m\xi - wt)]$, where m refers to the perturbation poloidal mode. Deriving a perturbed field (ex. $\tilde{F}$) with respect to y-coordinate yields:

$$\frac{\partial \tilde{F}(x,\xi)}{\partial y} = \frac{\partial \xi}{\partial y}\frac{\partial \tilde{F}(x,\xi)}{\partial \xi} = ik_y\tilde{F}(x,\xi) \qquad (1)$$

where $k_y = m/r_s$ is the fundamental harmonic for the mode perturbation in a slab. The periodicity of the perturbations in the y-direction allows us to write the perturbations as a complex Fourier series (example for the flux):

$$\widetilde{\psi}(x,\xi) = \sum_{k=-\infty}^{\infty} \psi_k(x)\exp^{imk\xi} \qquad (2)$$

where k is the Fourier harmonic number, $\psi_k(x)$ is a complex amplitude with x (radial) dependence. The dominant contribution of the perturbations is

the lowest resonant Fourier harmonic (i.e. k=1 and k=-1).

It is possible now to write the two linearised equations that will be time evolved in the numerical simulation:

$$\frac{\partial \psi_k}{\partial t} = -ik\frac{m}{r_s}\bar{v}_\xi \psi_k + ik\frac{m}{r_s}\varphi_k \frac{d\bar{\psi}}{dx} + \frac{\eta}{\mu_0}\left(\frac{\partial^2 \psi_k}{\partial x^2} - \left(k\frac{m}{r_s}\right)^2 \psi_k\right) \tag{3}$$

$$\frac{\partial \omega_k}{\partial t} = -ik\frac{m}{r_s}\varphi_k \frac{d^2\bar{v}_\xi}{dx^2} - ik\frac{m}{r_s}\bar{v}_\xi \omega_k - ik\frac{m}{\mu_0 \rho_0 r_s}\psi_k \frac{d\nabla^2\bar{\psi}}{dx} + ik\frac{m}{\mu_0\rho_0 r_s}\nabla^2\psi_k \frac{d\bar{\psi}}{dx} + \frac{\nu_0}{\rho_0}\left(\frac{\partial^2 \omega_k}{\partial x^2} - \left(k\frac{m}{r_s}\right)^2 \omega_k\right) \tag{4}$$

where the bar on ψ and v_ξ represent the preset equilibrium quantities with only a x-dependency.

In this work, two types of boundary conditions were chosen. The perfectly conducting wall (PCWBC) sets a plasma edge at x = ±L which in simple terms resembles a physical wall with infinite conductivity, where the radial perturbed magnetic field and velocity are zero. The equilibrium unstable fields for this set of boundary conditions was chosen such that the equilibrium magnetic field yields $B_{0y}(x) = |B|\tanh(x/L_B)$, and the helical magnetic flux ψ_0 will be the anti-derivative and the current density J_{0z} the derivative with respect to x. The Standard Boundary Conditions (SBC) doesn't have a plasma boundary. This means that in this model the profiles of the perturbed fields do not vanish at the boundaries. Therefore, the equilibrium helical flux is a Taylor expansion centred at x=0 given by $\psi_{eq}(x) \simeq x^2\psi_{eq}^{(2)}/2 + x^3\psi_{eq}^{(3)}/6 + x^4\psi_{eq}^{(4)}/24$. The most distinct feature of the SBC is the possibility of imposing the stability parameter at the boundaries by setting $\psi'_{|k|=1}(x = \pm L) \equiv \pm 0.5\Delta'_{BC}\psi_{|k|=1}(x = \pm L)$.

In the outer layer physics, resistivity and inertia are neglected and the tearing equation is obtained:

$$\nabla^2\psi_1 + \mu_0 \frac{dJ_{0z}(x)}{dx}\frac{1}{B_{0y}(x)}\psi_1 = 0 \tag{5}$$

The equation shows that the derivative of the solution has a discontinuity at the resonant surface x=0. Moreover, the solution of the tearing equation will depend on the equilibrium unstable fields, as well as the boundary conditions. The jump in the logarithmic derivative of ψ_1 at the resonant surface is the stability parameter, given by:

$$\Delta' = \frac{\psi_1'(0^+) - \psi_1'(0^-)}{\psi_1(0)} \tag{6}$$

where ψ_1' is the radial derivative of the perturbed magnetic flux. For the PCWBC case, the stability parameter can be derived analytically yielding $\Delta' = 2\,(1/k_y - k_y)$ for the PCWBC case, where here k_y is the normalized mode number and a growing mode (no other effects present) is obtained for $k_y < 1$. Furthermore, the perfect wall has an influence on the stability of the tearing mode. Figure 3 shows how varying the distance between the walls and the resonant surface affects the stability parameter. The varying quantity *scl_box* sets the distance of the walls in units of the current sheet width (thus constant L_B).

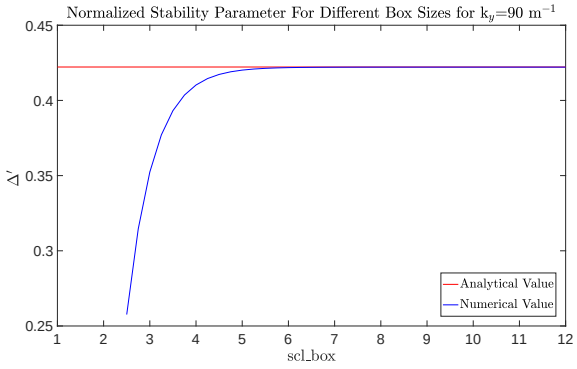

Figure 3: Numerical results of the stabilizing effect due to PCWBC for a perturbation mode k_y=90 m^{-1} and a current layer width L_B = 1 cm.

For the SBC case, the relation between the mode's stability parameter and Δ'_{BC}, k_y, and the width of the slab L is given by:

$$\Delta' = 2k_y \frac{k_y\left(1 - e^{2k_yL}\right) + 0.5\Delta'_{BC}\left(1 + e^{2k_yL}\right)}{k_y\left(1 + e^{2k_yL}\right) + 0.5\Delta'_{BC}\left(1 - e^{2k_yL}\right)} \tag{7}$$

The stability boundary ($\Delta' > 0$) is then given by $\Delta'_{BC} > 2k_y\ (e^{2k_yL}$ - 1)/(1 + e^{2k_yL}). The above expression is valid in the case of zero $\psi_{eq}^{(3)}$ and $\psi_{eq}^{(4)}$. Otherwise, a numerical code should be used to obtain the stability parameter of the mode.

IV. NUMERICAL PROGRAM

The numerical simulation code Ruth was originally written by J. Heres [14] and was further developed for this particular work. Substantial improvements were introduced in the code which will now be briefly discussed. A new set of boundary

conditions (PCWBC) was added and the equilibrium velocity terms were added to the time evolving equations. A routine which solves the tearing equation provides a suitable initial condition, reducing the amount of numerical effort to converge to the correct eigenfunctions. The non-linear terms are calculated by using Fast Fourier Transformations, which calculate these terms in real space and the result is transformed back to Fourier space and added to the linear terms. The problem regarding aliasing was corrected [15, Chapter 3.2.2]. The code initially time evolved the equations using a 4th order Runge-Kutta explicit method and the stability constraints regarding diffusive and convective terms had a severe impact on the efficiency of the code. Therefore, an adaptive time step was implemented (i.e. the time step will change every Runge-Kutta cycle to ensure stability) and the step double technique was chosen for this. Adaptive time step allows the user to set a tolerance for the acceptable error between time integration steps. Also, two semi-implicit time integration methods were added to the code which follow from the family of Runge-Kutta methods. The predictor corrector scheme is fourth order accurate in time, evaluating the equations four times, where the first and third are semi-implicit steps (predictor) and the second and fourth are explicit (corrector). The implicit-explicit Runge-Kutta method follows from the work of Ascher, Uri M et al [16]. For this method, the four-stage, third-order combination (4,4,3) instance was chosen. Four explicit and implicit steps are performed and the contributions of each step are added to yield a full time step. When implicit schemes are considered, it is necessary to solve linear system of equations (**Ax**=**b**) which is computationally quite demanding. Therefore, the Pardiso solver, from MKL library was chosen due to high-performance, robustness and memory efficiency, besides the several advantages over other tested solvers.

V. BENCHMARK

The tearing mode instability, first investigated by Furth, Killeen, and Rosenbluth [7] in a plane slab geometry was also used here and an eigenvalue problem for the flux perturbation resulted from the assumption that there was a perturbed component on the magnetic field growing exponentially in time. To solve the problem analytically, the plasma was divided into two regions: a narrow inner region where resistivity could not be neglected and an outer region, for which the solution is presented in equation (5). Coupling the two regions means setting the radial derivative of the perturbed magnetic flux at x=0 (Δ') in the boundary conditions of the tearing layer, since ($\delta_T \ll L$). The derived dispersion relation yields:

$$\gamma = \left(\frac{\Gamma(1/4)\Delta' L_B}{2\pi\Gamma(3/4)}\right)^{4/5} \tau_R^{-3/5} \left(\frac{\tau_A}{k_y L_B}\right)^{-2/5} \quad (8)$$

where $\tau_R = \mu_0 L_B^2/\eta$ is the resistive time, $\tau_A = L_B\sqrt{\mu_0\rho_0}/|B|$ is the Alfvén time and Γ here is the Gamma function. From the above equation, it is possible to conclude that the tearing instabilities grow on time-scales that are intermediate between the very short MHD time-scale τ_A and the much longer resistive time-scale τ_R. The tearing layer width is given by $\delta_T = 2\Delta' L_B \tau_R^{-1}\gamma^{-1}$. The numerical results are shown in Figure 4 for the PCWBC. The scaling between the growth rate γ and S is presented and the results agree with the theoretical dispersion relation. Another effect

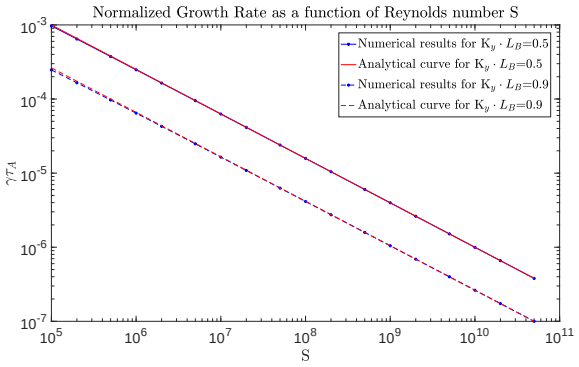

Figure 4: Normalised growth rate $\gamma\tau_A$ as a function of Reynold's number S, both in logarithmic scale. The points are the results from the numerical simulations and the lines represent the dispersion relation obtained from equation (8). It was considered two different values for the mode number k_y = 50 and 90 [m^{-1}], where L_B = 0.01 [m] and $\tau_A = 10^{-5}$ s.

was detected, concerning the effects of both the local gradient and the curvature (i.e. the second derivative) of the equilibrium current density distribution, which introduce corrections to the dispersion relation [17]. This effect is displayed in Figure 5. It is shown that as k_y decreases, the numerical growth rate starts to diverge from the theoretical predictions for lower values of S.

When finite viscosity is considered, the physics of the inner layer changes since the diffusive vis-

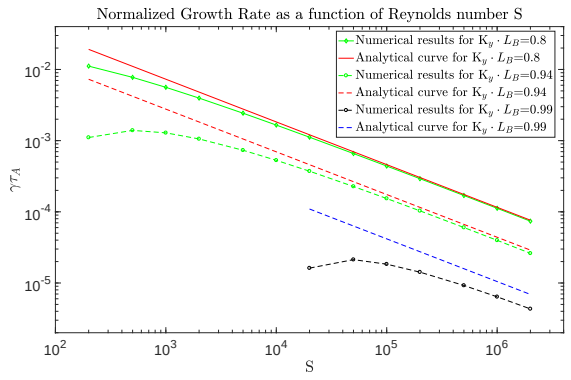

Figure 5: Normalised growth rate $\gamma\tau_A$ as a function of Reynold's number S, both in logarithmic scale. The points are the results from the numerical simulations and the lines represent the dispersion relation obtained from equation (8). It was considered three different values for the mode number k_y = 80, 94 and 99 [m^{-1}], where L_B = 0.01 [m] and $\tau_A = 10^{-5}$ s.

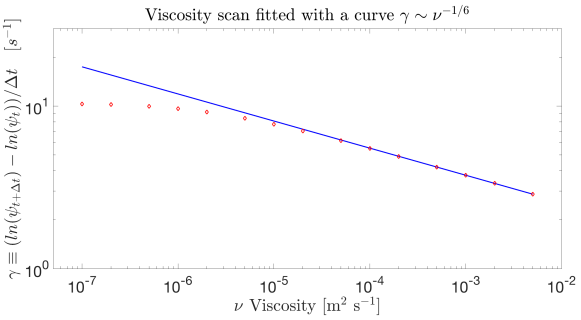

Figure 6: A scaling of the growth rate γ as a function of viscosity ν_0, both in logarithmic scale. The red diamonds are the numerically obtained growth rates and the blue line is the scaling $\gamma \propto \nu_0^{-1/6}$. It was considered an equilibrium with $\psi_{eq}^{(2)}$ = -0.5 × 10^6 s^{-1} ($\tau_A = 2 \times 10^{-6}$ s), mode number k_y = 1 [m^{-1}], L = 0.02 [m], Δ'_{BC} = 9.1274 [m^{-1}] and resistivity was set to $\eta = 5{\times}10^{-4}$ $m^2 s^{-1}$ ($\tau_R = 2 \times 10^3$ [s] → S=1 × 10^9).

cous term is added. Nevertheless, viscosity doesn't change the outer layer dynamics. The viscous time-scale is given by $\tau_v = \rho_0 L_B^2/\nu_0$ and a ratio between the resistive and viscous time-scales defines the Prandtl number: $\Gamma = \tau_R/\tau_V$. The dispersion relation for non-vanishing viscosity taken from Ref. [18] (where all drift related terms were neglected) yields:

$$w^5 \left[1 + \nu_0^{1/2} \frac{\Gamma(1/4) 2^{1/4} e^{i\frac{3\pi}{8}}}{\pi^{1/2}} \left(\frac{F(x)|B|}{\eta\rho_0} \right)^{\frac{1}{4}} w^{-\frac{3}{4}} \right] = i\gamma_T^5 \quad (9)$$

where γ_T is the dispersion relation for the inviscid tearing mode. In the limit $\nu_0 \to 0$ the inviscid dispersion relation is recovered $w = i\gamma_T$. From the above equation, non-vanishing viscosity reduces the dispersion relation by a factor $w \simeq i\gamma_T / \left(1 + a\,\nu_0^{1/2}\right)^{1/5}$, where a is a rough approximation to a constant. Physically, viscosity diffuses vorticity and consequently the current density, i.e. the flow vortices presented in Figure 2 are damped. Furthermore, F. Porcelli [19] studied the modifications to the dispersion relation when viscous effects dominate. The author found that the growth rate scaled $\gamma \propto \eta^{5/6} \nu_0^{-1/6} \Delta'^{-1}$. In Figure 6 the numerical results are shown, where the scaling with viscosity is verified. It is possible to conclude that the perturbation enters the visco-tearing regime for a Prandtl number of the order of $\Gamma \sim 10^{-2}$. Viscosity reduces the growth rate of the mode but doesn't completely stabilize the mode.

VI. EFFECTS OF SHEAR FLOW

In the present chapter, the effects of equilibrium plasma flow on the stability of tearing modes is analysed. A brief literature review centred on the linear evolution of the mode follows:

An analytical investigation of this effect in slab geometry was performed by Chen and Morrison [20]. They found that shear flow changes the dynamics of the outer and inner layer. Thus the tearing equation (5) no longer holds and the stability parameter Δ' can change drastically. In the inner layer, the tearing mode is expected to be sensitive to the derivative of the equilibrium plasma velocity at x=0. Therefore, the authors considered the ratio of the derivatives of the plasma flow to the magnetic field, both at x=0, for three scenarios: a very small ratio ($\ll 1$), comparable ratio ($\lesssim 1$) and a ratio above one (>1). In the first case, the static tearing mode scaling $\gamma \propto S^{-3/5}$ is recovered. However, the tearing mode is destabilized due to the destabilizing effect in the outer layer. For the second case, the scaling is changed to $\gamma \propto S^{-1/2}$ and the condition for growing modes $\Delta' > 0$ is removed. In the third case, the tearing mode is stabilized due to the freezing of the flow to the magnetic field. Moreover, shear flow can also drive Kelvin-Helmholtz instabilities.

The same authors have included viscous effect on the previous work [21]. The same ratio is considered and the analysis follows for the same scenarios. As in the inviscid analysis, a very small ratio ($\ll 1$) only accounts for the destabilizing effect on the outer layer. For comparable ratio ($\lesssim 1$) and for comparable resistive and viscous time-scales, the condi-

tion for growing modes $\Delta' > 0$ is restored. Moreover, when the ratio between shears becomes closer to unity, the growth rate decreases and for a ratio above unity, the tearing instability is totally suppressed. For a viscous time-scale lower than the resistive time-scale, the growth rate of the tearing mode is enhanced.

Ofman et al performed numerical simulations and compared the results with the findings of the previous papers [22]. A good agreement with the analytical growth rate scalings was found.

The PCWBC was chosen to be used for this investigation. Thus the equilibrium plasma velocity profile follows:

$$\bar{v}_{0y}(x) = v_{eq} + v_{shear} \tanh\left(\frac{x}{L_v}\right) \qquad (10)$$

where v_{shear} is the velocity amplitude ($\Delta\bar{v}_{0y} = 2v_{shear}$) and L_v is the velocity shear layer width (i.e. the half of the radial width where the transition from $\pm v_{shear}$ occurs).

When a constant equilibrium flow is considered, the magnetic island will move in the y-direction at a constant velocity v_{eq}. By applying a variable change to the growth rate $\gamma \to \gamma + ik_y v_{eq}$, the dispersion relation yields the same result as presented in equation (8). Therefore, a constant velocity is simply a Doppler shift of the static solution to the constant moving frame of the rotating plasma.

For a sheared equilibrium plasma velocity, due to the radial dependency, the system of eigenfunctions would have multiple eigenvalues at different points in the radial grid. Therefore, a numerical code is necessary to test whether the system of equations can converge to a single eigenvalue problem. For an inviscid plasma, Figure 7 shows the growth rate for different normalized velocity shear layer L_v to the current sheet layer L_B and the four curves were taken for different plasma velocity amplitudes $v_{shear} < 0.01 v_A$ - Mach number below 1%. The destabilizing effect of shear flow in the inviscid case agree with the conclusions found in the literature and the results are similar to Figure 6 in article [22] for the tanh profile. Furthermore, by displaying the results for different plasma velocity amplitudes v_{shear} and in the case $L_v/L_B \to 4$, the growth rate increases with the amplitude, leads to the conclusion that shear destabilizes the tearing mode in the outer layer, thus changing the stability parameter Δ'. On the other hand, when $L_v/L_B \to 0$, the destabilizing effect of shear flow is reduced, which might suggest that shear flow has a stabilizing effect in the inner layer. The reversal of the destabilizing trend occurs for lower shear layer widths as the plasma velocity amplitude decreases. This could be related to the fact that the tearing layer width decreases with the stability parameter $\delta \propto \Delta'$ and the stabilizing effect in the inner layer should be more pronounced as the tearing layer width is increased in size.

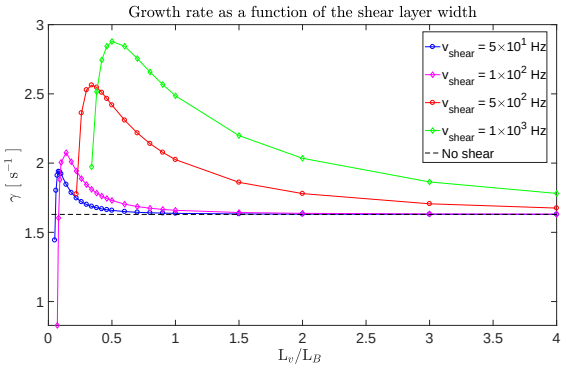

Figure 7: A scaling of the growth rate γ as a function of the shear layer width L_v normalized to the current sheet width L_B. The data points were obtained for a Lundquist number S = 10^7, k_y=90 [m^{-1}], L_B=1 [cm], scl_box = 11 (no stabilizing effect from the perfect wall BC is present). The diamonds correspond to the growth rates obtained by numerical simulations and the lines join the diamonds. The dashed curve was also obtained numerically when shear flow is not present.

Viscous effects were also considered for three Prandtl numbers $\Gamma = 5 \times 10^{-2}$, 1×10^0 and 1×10^2. Figures 8, 9 and 10 show the same scaling of the growth rate as in Figure 7. In all Figures, the data points were obtained for a Lundquist number S = 10^7, k_y=90 [m^{-1}], L_B=1 [cm] and scl_box = 11 (no stabilizing effect from the perfect wall BC is present).

In the case $\Gamma = 5 \times 10^{-2}$ it is observed that for normalized velocity shear layer widths $L_v/L_B < 0.8$, increasing the plasma velocity amplitude results in a stabilizing effect of the mode. The same behaviour is observed in the $\Gamma = 1 \times 10^0$ and $\Gamma = 1 \times 10^2$ cases for $L_v/L_B < 1$ and $L_v/L_B < 0.5$, respectively. The threshold of L_v/L_B to a stabilizing effect appears to increase when going from an inviscid plasma to a plasma where resistive diffusion is the same as the viscosity diffusion, and decreases when viscosity is further increased. These results contrasts the findings of some of the authors [20, 23] where it was reasonably established that velocity gradients always had qualitatively the same effect on the mode stability. This likely results from the assumption that the shear layer width is always assumed to be the

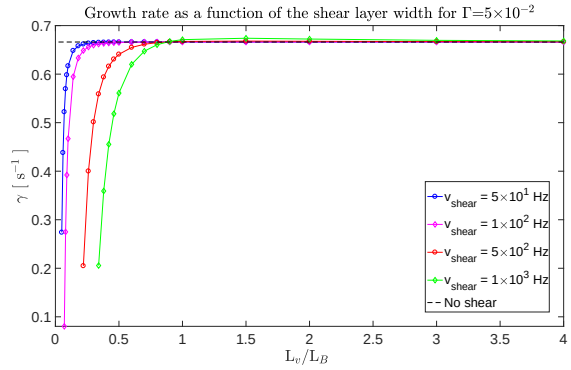

Figure 8: A scaling of the growth rate γ as a function of the shear layer width L_v normalized to the current sheet width L_B for $\Gamma = 5{\times}10^{-2}$. The diamonds correspond to the growth rates obtained by numerical simulations and the lines join the diamonds. The dashed curve was also obtained numerically when shear flow is not present.

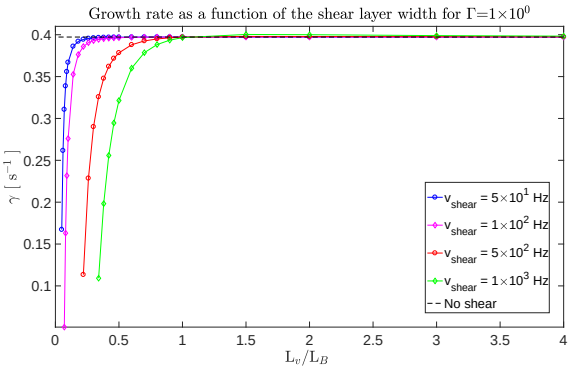

Figure 9: A scaling of the growth rate γ as a function c the shear layer width L_v normalized to the current shee width L_B for $\Gamma = 1{\times}10^{0}$. The diamonds correspond t the growth rates obtained by numerical simulations an the lines join the diamonds. The dashed curve was als obtained numerically when shear flow is not present.

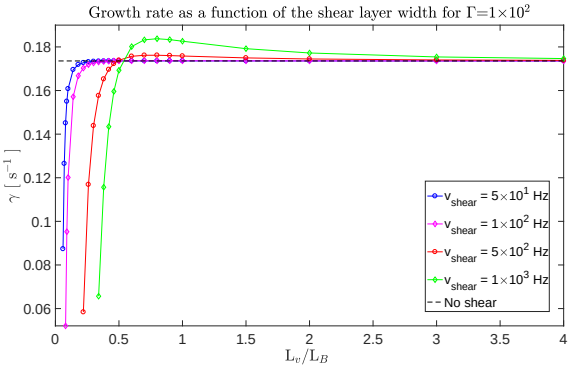

Figure 10: A scaling of the growth rate γ as a function of the shear layer width L_v normalized to the current sheet width L_B for $\Gamma = 1{\times}10^{2}$. The diamonds correspond to the growth rates obtained by numerical simulations and the lines join the diamonds. The dashed curve was also obtained numerically when shear flow is not present.

same, i.e. velocity shear is controlled solely through the differential rotation.

A stable mode was considered for this analyses by changing the mode number to k_y=102 [m^{-1}], L_B=0.01 [m] and a Prandtl number of $\Gamma = 1 \times 10^{-2}$ (close to the inviscid plasma regime). The selected mode number yields a negative stability parameter ($\Delta' = -7.92 \times 10^{-2}$), implying a marginally stable regime for the static tearing mode. Figure 11 shows the growth rate as a function of the plasma velocity amplitude v_{shear} for a fixed velocity shear layer width L_v=L_B=1 [cm]. The growth rates obtained were always negative and a growing mode was not detected. Therefore, one concludes that the condition $\Delta' > 0$ for a growing mode is maintained in the presence of shear flow for an inviscid plasma. This result contradicts the findings of Chen and Morrison in [20]. A more detailed investigation should be performed to access if the same results are obtained for other values of Prandtl number and velocity shear layer width.

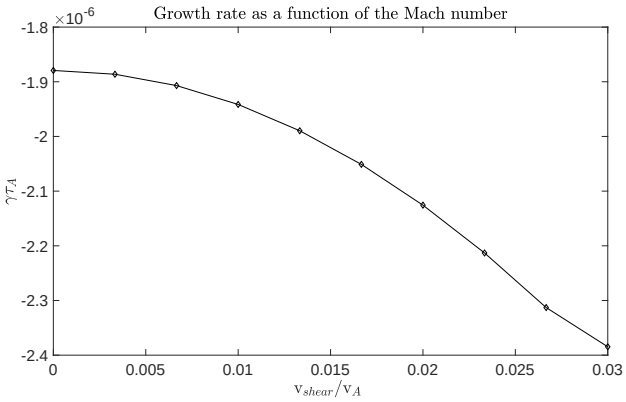

Figure 11: A scaling of the numerical normalized growth rate $\gamma\tau_A$ as a function of the Mach number v_{shear}/v_A for $\Gamma = 1{\times}10^{-2}$ and scl_box = 5 was used.

VII. CONCLUSIONS

Overall, the effect of sheared flow strongly depends on the ratio of the widths of the sheared velocity layer and the the plasma current density channel. In fact, while for a large ratio the sheared flow is typically destabilizing, as soon as the flow shear layer becomes significantly smaller than the plasma current channel width, the tearing mode starts to be increasingly stabilized as the differential rotation at both sides of the rational surface increases. This pattern is observed at all viscous regimes. One can nonetheless stress that the destabilizing/stabilizing effect of shear flow is much more

notorious in the two limiting viscous cases i.e. inviscid and strongly viscous plasma. The destabilizing effect on strongly viscous plasma scenario is particularly striking since, contrary to the normal classical tearing mode in static plasmas, viscosity (usually a stabilizing effect) can in fact assist to a destabilising contribution, in the the presence of shear flow. Also the results shown suggests that shear flow has a destabilizing effect in the outer layer (due to the inclusion of inertial terms in the tearing equation, changing the stability parameter) and a stabilizing effect on the inner layer. An intuitive interpretation relies on the extent of sheared plasma flow that is seen on the outer ideal region: the smaller the shear layer width, the smaller this extent is and thus only inner layer physics is relevant. On the contrary, for larger flow shear width, a sizeable velocity gradient is seen over the entire ideal region whereas limited shear is concentrated at the inner layer. The results are in agreement with previous works by previous authors but are more complete since, in this thesis and contrary to those works, the velocity gradients at the rational surface can either be due to varying velocity shear layer width and differential velocity.

---

[1] Alexander P. Mathews. Renewable energy technologies: Panacea for world energy security and climate change? *Procedia Computer Science*, 32:731–737, 2014.

[2] Jeffrey P Freidberg. *Plasma physics and fusion energy*. Cambridge university press, 2008.

[3] John Wesson and David J Campbell. *Tokamaks*. Oxford University Press, 3rd edition, 2004.

[4] S.P. Hirshman and D.J. Sigmar. Neoclassical transport of impurities in tokamak plasmas REVIEW PAPER NEOCLASSICAL TRANSPORT OF IMPURITIES United States of America. *Nuclear Fusion*, 21(9):1079–1201, 1981.

[5] P H Rutherford. Nonlinear growth of the tearing mode. *Physics of Fluids*, 16(11):1903, 1973.

[6] R. B. White. Resistive reconnection. *Reviews of Modern Physics*, 58(1):183, 1986.

[7] Harold P Furth, John Killeen, and Marshall N Rosenbluth. Finite-Resistivity Instabilities of a Sheet Pinch. *Physics of Fluids*, 6(4):459, 1963.

[8] R Fitzpatrick. Interaction of tearing modes with external structures in cylindrical geometry (plasma). *Nuclear Fusion*, 33(7):1049, 1993.

[9] P. C. De Vries, M. F. Johnson, B. Alper, P. Buratti, T. C. Hender, H. R. Koslowski, and V. Riccardo. Survey of disruption causes at JET. *Nuclear Fusion*, 51(5), 2011.

[10] M F F Nave, R Coelho, E Lazzaro, and F Serra. The influence of mode coupling on the non-linear evolution of tearing modes. *The European Physical Journal D-Atomic, Molecular, Optical and Plasma Physics*, 8(2):287–297, 2000.

[11] Hinrich Lütjens, Jean-François Luciani, and Xavier Garbet. Curvature effects on the dynamics of tearing modes in tokamaks. *Physics of Plasmas*, 8(10):4267–4270, 2001.

[12] Richard Fitzpatrick. Helical temperature perturbations associated with tearing modes in tokamak plasmas. *Physics of Plasmas*, 2(3):825–838, 1995.

[13] E. Westerhof. Letters: Tearing mode stabilization by local current density perturbations. *Nuclear Fusion*, 30(6):1143–1147, 1990.

[14] Jacco Heres. *2D theory and simulations of Neoclassical Tearing Modes*. PhD thesis, Utrecht University, 2013.

[15] C Canuto. *Spectral methods in fluid dynamics*. Springer series in computational physics. Springer-Verlag, 1988.

[16] Uri M Ascher, Steven J Ruuth, and Raymond J Spiteri. Implicit-explicit Runge-Kutta methods for time-dependent partial differential equations. *Applied Numerical Mathematics*, 25(2):151–167, 1997.

[17] F. Militello, G. Huysmans, M. Ottaviani, and F. Porcelli. Effects of local features of the equilibrium current density profile on linear tearing modes. *Physics of Plasmas*, 11(1):125–128, 2004.

[18] E. Lazzaro, G. Lampis, and A. Bernardinello. Effects of Nonvanishing Ion Viscosity on the Linear Stability of Drift Tearing Modes in a Tokamak. *Journal of the Physical Society of Japan*, 63(12):4373–4378, 1994.

[19] Francesco Porcelli. Viscous resistive magnetic reconnection. *Physics of Fluids*, 30(6):1734, 1987.

[20] X. L. Chen and P. J. Morrison. Resistive tearing instability with equilibrium shear flow. *Physics of Fluids B: Plasma Physics*, 2(3):495–507, 1990.

[21] X. L. Chen and P. J. Morrison. The effect of viscosity on the resistive tearing mode with the presence of shear flow. *Physics of Fluids B*, 2(11):2575–2580, 1990.

[22] L Ofman, X L Chen, P J Morrison, and R S Steinolfson. Resistive tearing mode instability with shear flow and viscosity. *Physics of Fluids B: Plasma Physics*, 3(6):1364–1373, 1991.

[23] R Coelho and E Lazzaro. Effect of sheared equilibrium plasma rotation on the classical tearing mode in a cylindrical geometry. *Physics of Plasmas*, 14(1):12101, 2007.